Supplementary Information

Nanoscale crystallization of a low band gap polymer in printed titania mesopores

Nian Li[1], Lin Song[1,2], Nuri Hohn[1], Nitin Saxena[1], Wei Cao[1], Xinyu Jiang[1] and Peter Müller-Buschbaum[1,3]

[1] Technische Universität München, Physik-Department, Lehrstuhl für Funktionelle Materialien, James-Franck-Str. 1, 85748 Garching, Germany

[2] Institute of Flexible Electronics (IFE), Northwestern Polytechnical University (NPU), Youyixilu 127, Xi'an 710072, Shaanxi, China

[3] Heinz Maier-Leibnitz Zentrum (MLZ), Technische Universität München, Lichtenbergstr. 1, 85748 Garching, Germany
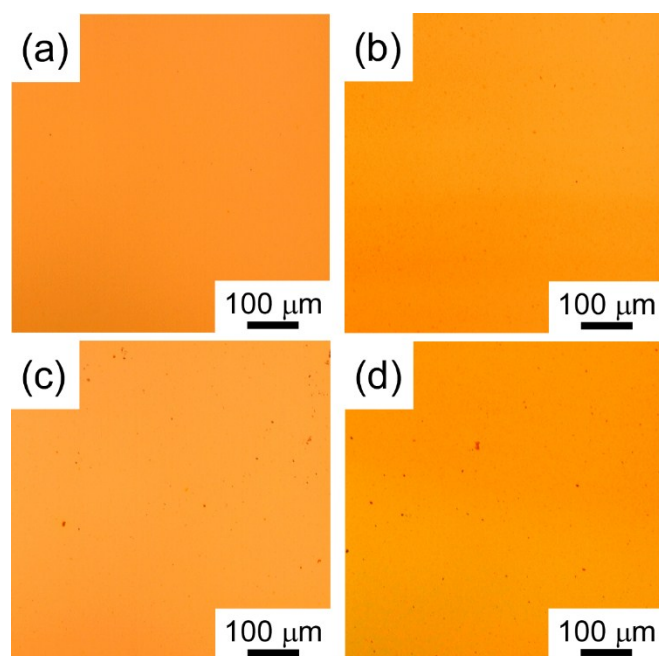
Figure S1. Optical microscopy images of the mesoporous titania films deposited by printing from solutions containing different weight fractions of TTIP: w_{TTIP} of (a) 1.5%, (b) 2.0%, (c) 2.5% and (d) 3.0%.
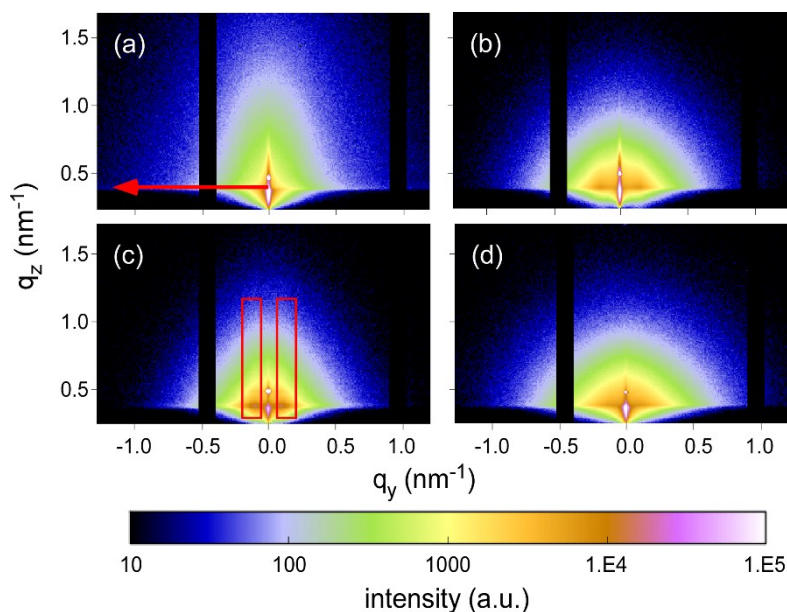
Figure S2. 2D GISAXS data of the mesoporous titania films deposited by printing after calcination and cast from solution with different w_{TTIP} values of (a) 1.5%, (b) 2.0%, (c) 2.5% and (d) 3.0%. The red arrow in (a) indicates the exemplary position where the horizontal line cuts are performed. The red rectangles in (c) indicate two vertical Bragg scattering rods. All the images are in the same intensity scale.

GISAXS data and modeling

GISAXS is a powerful tool to detect the inner structures buried in thin films and allows for the determination of structural length scales ranging from nanometer to micrometer with a high statistical relevance. Figure S2 displays the 2D data from the GISAXS measurements performed on printed titania films deposited by printing from solutions with different w_{TTIP}. To avoid oversaturation of the detector, a circular beamstop is used to shield the specular reflected X-ray beam which occurs at the exit angle equal to the incident angle. The maximum intensity is located in the material dependent Yoneda peak region,[1] which is correlated to the critical angle of titania. For a quantitative analysis, the horizontal line cuts as marked by the red arrow in Figure S2a are done at the titania Yoneda peak position along the q_y direction using the DPDAK software.[2] The horizontal line cuts enable us to obtain the lateral structural information of the probed titania films. To retrieve more details about the lateral structures, the cuts are modelled in the framework of the Distorted Wave Born Approximation (DWBA) using the Local Monodisperse Approximation (LMA) as well as the Effective Interface Approximation (EIA).[3–6] Thus, the differential cross section is simplified to

$$\frac{d\sigma}{d\Omega} = \frac{A\pi^2}{\lambda^4}(1-n^2)^2|T_i|^2|T_f|^2 P(\vec{q}) \propto P(\vec{q})$$

where A is the illuminated area, λ is the wavelength, n is the refractive index, $T_{i,f}$ are the Fresnel-transmissivities of the incoming and outgoing beams, $P(\vec{q})$ is the diffuse scattering factor. The diffuse scattering factor can be approximated by

$$P(\vec{q}) \propto N|F(\vec{q})|^2 S(\vec{q})$$

where N is the number of scattering objects, $F(\vec{q})$ the form factor and $S(\vec{q})$ the structure factor. The scattering objects with a certain shape and size are referred to as the form factors, originating from the foam-like titania nanostructure. Due to insights from SEM, the scattering objects are assumed to have a cylindrical shape with a Gaussian distributed size, which is a commonly applied model for mesoporous TiO_2 films.[7,8] The center-to-center distances between the neighboring objects are referred to as the structure factors. More details about the fitting model can be found in our previous work.[9] In the present model, three characteristic structure and form factors are needed to model the horizontal line cuts. Modelling results are shown as the red solid lines in Figure 3a. The pore size in average is approximated by

Pore size = (center-to-center distance between nanoparticles – 2 × nanoparticle radius).

Thus, the radii and pore sizes of foam-like titania films can be quantitatively extracted from GISAXS measurements.
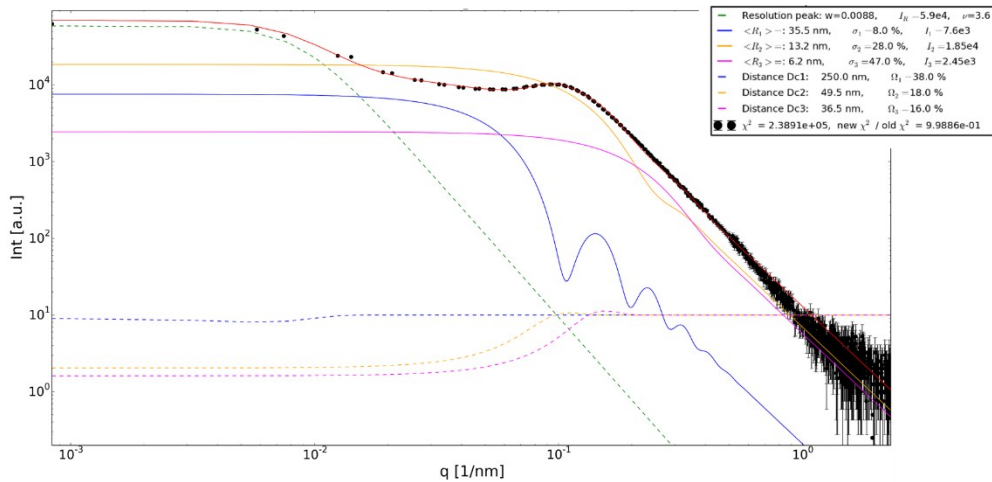
Figure S3. Example of the applied GISAXS modelling of the intensity in a horizontal line cut of the 2D GISAXS data with the model as explained in the text.

Estimation of volume distribution of the modeled structures[10]

Within the LMA the location and kind of scattering centers are correlated and the scattering intensity is

$$I(\vec{q}) \propto \sum_i N_i \cdot \langle |F(q,R_i)|^2 \rangle \cdot S(\vec{q},R_i)$$

Considering that cylinders have different radii R_i but equal height, and $S(\vec{q},R_i,\rho) \rightarrow 1$ for an uncorrelated distribution of scattering objects and $F(\vec{q},R_i)$ being the form factor of cylinders.[6]

To calculate the mean square of the form factors, it is weighted with $w_i(R)$ and normalized. $w_i(R)$ represents a Gaussian distribution.

$$\langle |F(q,R_i)|^2 \rangle = \frac{\int w_i(R)|F(q,R)|^2 dR}{\int w_i(R)dR}$$

Thus, a dependence for the spectrum of radii R can be obtained.

$$I(\vec{q}) \propto \int \left(\sum_i N_i \cdot w_i(R) \right) \cdot |F(q,R)|^2 dR$$

The distribution of the modeled structures inside the film can be represented as a superposition of form factor functions versus their intensity. However, the intensity scales is linear with the number N_i of scattering objects and radii R_i, so that volume fractions are estimated by

$$v = \frac{N_2 \cdot V_2}{N_2 \cdot V_2 + N_1 \cdot V_1}$$

$$\frac{V_1}{V_2} = \frac{\pi H \langle R_1 \rangle^2}{\pi H \langle R_2 \rangle^2}$$
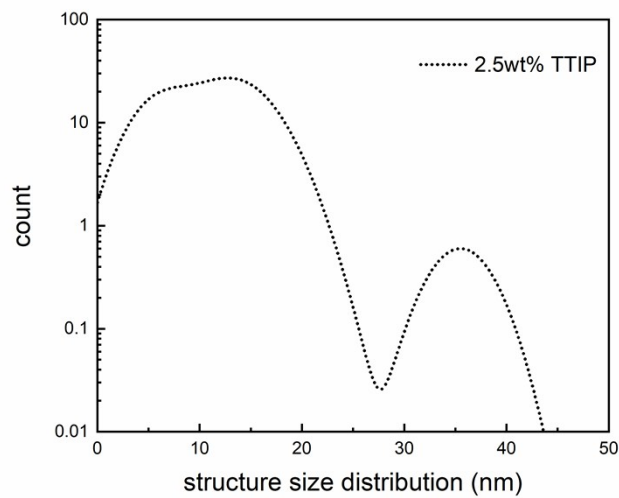
Figure S4. An example of structure size distribution given by the superposition of the Gaussian distribution for the three form factors extracted from the modelling.
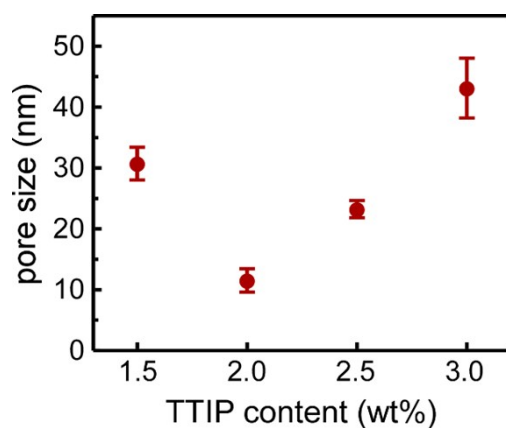
Figure S5. Extracted characteristic length scales: pore size in the printed titania thin films as a function of w_{TTIP}. Red circles represent middle-sized structures.

Table S1. Characterization of P3HT and PffBT4T-2OD used in this study

	molecular weight M_w (g mol^{-1})	solubility/processing solvents
P3HT	65,200	chlorobenzene, toluene, etc at room temperature[11,12]
PffBT4T-2OD	131,000	dichlorobenzene or chlorobenzene + dichlorobenzene (1:1 v/v) at elevated temperature ca. 110 °C[13]
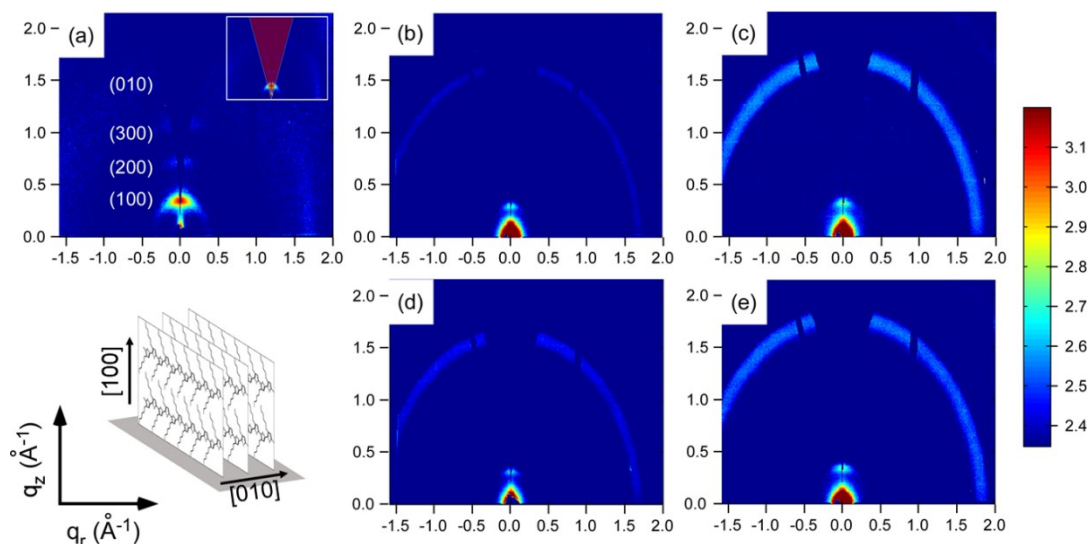
Figure S6. 2D GIWAXS data of (a) a pure P3HT reference sample the P3HT-backfilled titania films deposited by printing from solutions with different TTIP weight fractions: (b) 1.5%, (c) 2.0%, (d) 2.5% and (e) 3.0%. For all samples, the azimuthally integrals are done from -15° to 15° (vertical direction) to extract quantitative information about edge-on oriented P3HT crystals. The performed cake cuts are as shown in the inset of panel (a). The schematic (left corner) shows an edge-on oriented P3HT crystal with the lamellar stacking in [100] direction and the $\pi-\pi$ stacking in [010] direction.
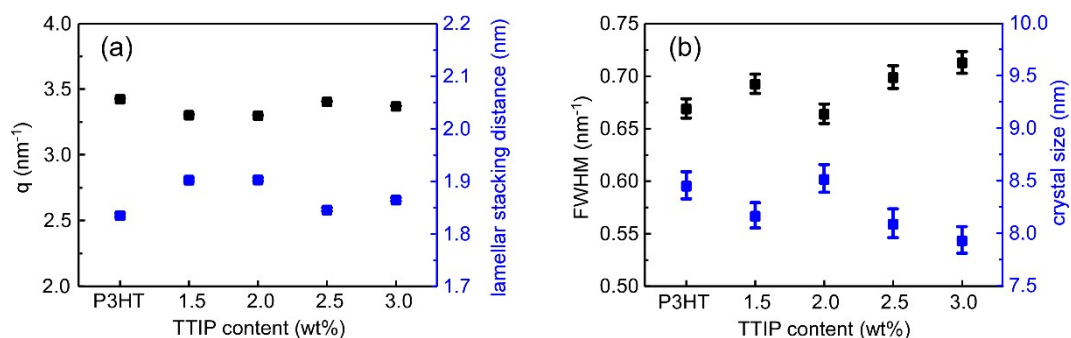
Figure S7. (a) q-positions of P3HT (100) Bragg peak and the corresponding lamellar stacking distances, and (b) related FWHM values and the calculated crystal sizes using the Scherrer equation as extracted from the GIWAXS measurements of the active layers as a function of w_{TTIP}. A pure P3HT sample is prepared as a reference.

The crystallite size can be calculated by

$$\left(\varepsilon_{obs} - \varepsilon_{instr}\right) = \frac{K\lambda}{D_{hkl}cos\theta} + 4\varepsilon_{str}tan\theta$$

where ε_{obs} is the line width, ε_{instr} is the instrumental broadening, K is the Scherrer constant (= 0.9), λ is the X-ray wavelength, D_{hkl} is the crystallite size and ε_{str} is the strain. Considering the fact that the instrumental broadening and strain are much lower than the actual line broadening, they can be neglected,[14] thereby the crystal sizes obtained by

$$D_{hkl} = \frac{K\lambda}{FWHM \cdot cos\theta}$$
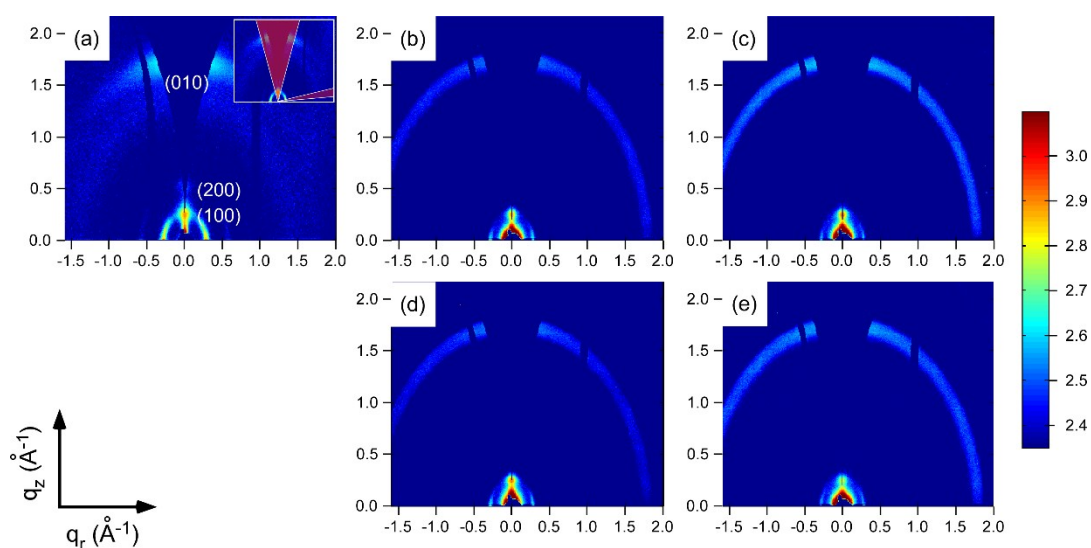
Figure S8. 2D GIWAXS data of (a) a pure PffBT4T-2OD reference sample and the PffBT4T-2OD-backfilled titania films deposited by printing from solutions with different TTIP weight fractions: (b) 1.5%, (c) 2.0%, (d) 2.5% and (e) 3.0%. For all samples, the azimuthally integrals are done from -15° to 15° (vertical direction) and 75° to 85° (horizontal direction) to extract quantitative information about the edge-on and face-on oriented PffBT4T-2OD crystals, respectively. The performed cake cuts are as shown in the inset of panel (a).
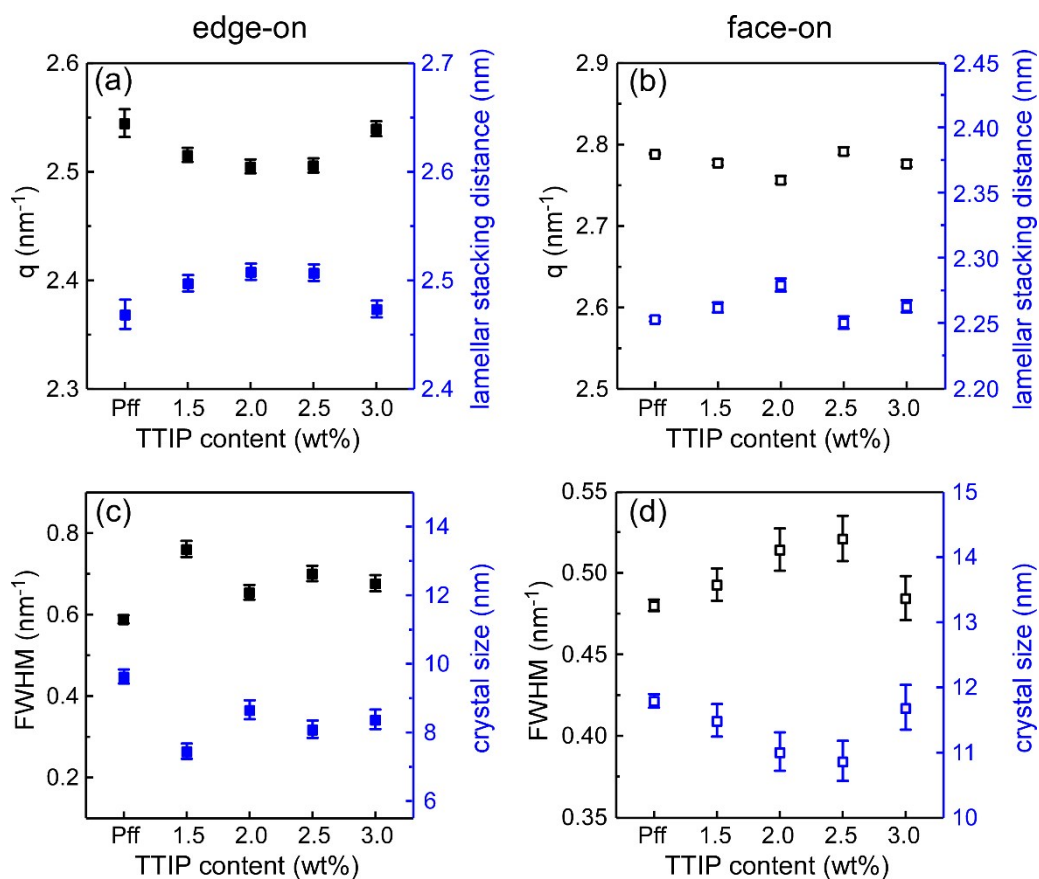
Figure S9. q-positions of PffBT4T-2OD (100) Bragg peak and the corresponding lamellar stacking distances in (a) edge-on direction and (b) face-on direction, and related FWHM values and calculated crystal sizes using Scherrer equation in (c) edge-on direction and (d) face-on direction extracted from GIWAXS measurements of the active layers as a function of w_{TTIP}. A pure PffBT4T-2OD sample is prepared as a reference.
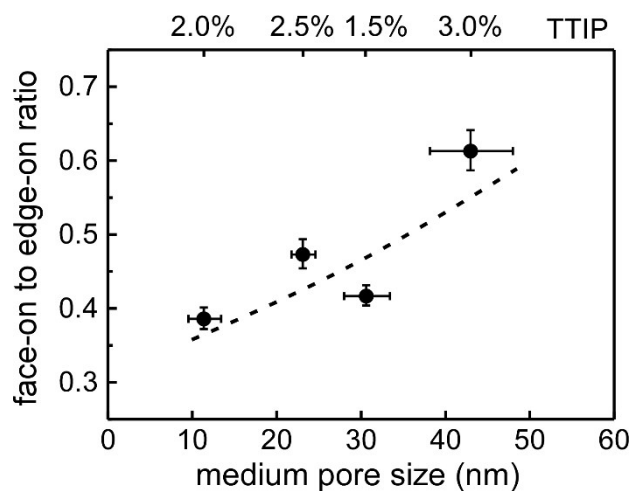
Figure S10. Face-on to edge-on ratio of PffBT4T-2OD (100) Bragg peak as function of the printed titania pore size. The area ratio of the PffBT4T-2OD (100) Bragg peaks is compared in in-plane and out-of-plane directions. This index is used to quantify the ratio between face-on orientated to edge-on orientated PffBT4T-2OD crystallites.

References

1   Y. Yoneda, *Phys. Rev.*, 1963, **131**, 2010–2013.

2   G. Benecke, W. Wagermaier, C. Li, M. Schwartzkopf, G. Flucke, R. Hoerth, I. Zizak, M. Burghammer, E. Metwalli, P. Müller-Buschbaum, M. Trebbin, S. Förster, O. Paris, S. V. Roth and P. Fratzl, *J. Appl. Crystallogr.*, 2014, **47**, 1797–1803.

3   G. H. Vineyard, *Phys. Rev. B*, 1982, **26**, 4146–4159.

4   S. K. Sinha, E. B. Sirota and S. Garoff, *Phys. Rev. B*, 1988, **38**, 2297–2311.

5   M. Rauscher, T. Salditt and H. Spohn, *Phys. Rev. B*, 1995, **52**, 16855–16863.

6   R. Lazzari, *J. Appl. Crystallogr.*, 2002, **35**, 406–421.

7   L. Song, W. Wang, V. Körstgens, D. Moseguí González, F. C. Löhrer, C. J. Schaffer, J. Schlipf, K. Peters, T. Bein, D. Fattakhova-Rohlfing, S. V. Roth and P. Müller-Buschbaum, *Nano Energy*, 2017, **40**, 317–326.

8   N. Hohn, S. J. Schlosser, L. Bießmann, S. Grott, S. Xia, K. Wang, M. Schwartzkopf, S. V. Roth and P. Müller-Buschbaum, *Nanoscale*, 2018, **10**, 5325–5334.

9   L. Song, W. Wang, S. Pröller, D. Moseguí González, J. Schlipf, C. J. Schaffer, K. Peters, E. M.

Herzig, S. Bernstorff, T. Bein, D. Fattakhova-Rohlfing and P. Müller-Buschbaum, *ACS Energy Lett.*, 2017, **2**, 991–997.

10   J. Schlipf, P. Docampo, C. J. Schaffer, V. Körstgens, L. Bießmann, F. Hanusch, N. Giesbrecht, S. Bernstorff, T. Bein and P. Müller-Buschbaum, *J. Phys. Chem. Lett.*, 2015, **6**, 1265–1269.

11   M. Rawolle, K. Sarkar, M. A. Niedermeier, M. Schindler, P. Lellig, J. S. Gutmann, J. F. Moulin, M. Haese-Seiller, A. S. Wochnik, C. Scheu and P. Müller-Buschbaum, *ACS Appl. Mater. Interfaces*, 2013, **5**, 719–729.

12   L. Song, W. Wang, V. Körstgens, D. Moseguí González, Y. Yao, N. K. Minar, J. M. Feckl, K. Peters, T. Bein, D. Fattakhova-Rohlfing, G. Santoro, S. V. Roth and P. Müller-Buschbaum, *Adv. Funct. Mater.*, 2016, **26**, 1498–1506.

13   Y. Liu, J. Zhao, Z. Li, C. Mu, W. Ma, H. Hu, K. Jiang, H. Lin, H. Ade and H. Yan, *Nat. Commun.*, 2014, **5**, 1–8.

14   K. Juraic, D. Gracin, B. Santic, D. Meljanac, N. Zoric, A. Gajovic, P. Dubcek, S. Bernstorff and M. Ceh, *Nucl. Instruments Methods Phys. Res. B*, 2010, **268**, 259–262.